The effect of zirconia content on the structure of zirconia-silica xerogels as determined by x-ray and neutron diffraction and Zr K-edge EXAFS and XANES

2000 J. Phys.: Condens. Matter 12 3505

(http://iopscience.iop.org/0953-8984/12/15/301)

J. Phys.: Condens. Matter **12** (2000) 3505–3519. Printed in the UK PII: S0953-8984(00)05035-9

The effect of zirconia content on the structure of zirconia–silica xerogels as determined by x-ray and neutron diffraction and Zr K-edge EXAFS and XANES

G Mountjoy†, R Anderson†, R J Newport† and M E Smith‡

† School of Physical Sciences, The University of Kent at Canterbury, Canterbury CT2 7NR, UK
‡ Department of Physics, Warwick University, Coventry CV4 7AL, UK

E-mail: g.mountjoy@ukc.ac.uk, r.j.newport@ukc.ac.uk and m.e.smith1@warwick.ac.uk

Received 8 June 1999, in final form 7 February 2000

Abstract. We present combined x-ray and neutron diffraction, and extended x-ray absorption fine structure (EXAFS) and x-ray absorption near edge structure (XANES) results on a single set of $(ZrO_2)_x(SiO_2)_{1-x}$ xerogel samples. In these samples, there is improved homogeneity of Zr compared to our previous study, due to greater dilution of the precursor Zr n-propoxide in propan-1-ol. Structural parameters obtained from model fitting of the diffraction and EXAFS data are compared with those in reference compounds. A qualitative comparison of XANES spectra is also made. The results show that for $x \geqslant 0.3$ there is phase separation of ZrO_2 and the Zr environment is similar to that in monoclinic ZrO_2 and Zr hydroxide. For $x \leqslant 0.2$ there is no phase separation, the SiO_2 network is distorted and the Zr coordination is similar to that in Zr n-propoxide, with some Zr–Zr clustering.

1. Introduction

Zirconia (ZrO_2) is a useful material because it has high fracture toughness, mechanical strength and chemical durability, and it exhibits significant ionic conductivity at elevated temperatures. Zirconia–silica materials can be used as coatings, fibres, catalysts and high-refractive-index glasses. The refractive index increases as the ZrO_2 content increases [1], as does the resistance to alkaline conditions [2]. The strength and hardness of zirconia–silica materials also increase with ZrO_2 content [1]. There is one mixed ZrO_2–SiO_2 crystalline compound, zircon ($ZrSiO_4$), but its formation requires heating at 1400 °C [3]. ZrO_2–SiO_2 glasses with significant ZrO_2 content are difficult to produce using conventional melt–quench techniques due to the extremely high temperatures required [4].

Sol–gel processing [5] offers a technique for producing ZrO_2–SiO_2 glasses with large ZrO_2 content, but without the need for very high processing temperatures. In the majority of cases, Zr and Si alkoxides are used as precursors and a gel is formed by the hydrolysis and condensation of the alkoxides. The gel is then dried to produce an amorphous, porous, hydrated solid called a xerogel. In $(ZrO_2)_x(SiO_2)_{1-x}$ xerogels, Zr is expected to act as a network modifier. Substitution of Zr for Si in the SiO_2 network is unfavourable because the Zr^{4+} ion has a large size and coordination number (i.e. 6–8) [6]. Phase separation of ZrO_2 can occur in ZrO_2–SiO_2 xerogels and the extent of phase separation depends on the composition and preparation method.

0953-8984/00/153505+15$30.00

The atomic structure of amorphous $(ZrO_2)_x(SiO_2)_{1-x}$ xerogels has been investigated using several techniques. IR [7, 8], Raman [7] and ^{29}Si NMR [8] studies show that Zr disrupts the SiO_2 network. ^{17}O NMR studies [8] for $x = 0.1$ show a predominance of Si–O–Zr oxygen configurations, whilst for $x = 0.4$ they show significant amounts of O–Zr_n configurations, i.e. corresponding to phase separation of ZrO_2, which are similar to those in monoclinic ZrO_2 (m-ZrO_2 [9]). For $x < 0.1$, IR and Raman studies [7] have concluded that the Zr nearest-neighbour environment is like that in cubic ZrO_2 (c-ZrO_2 [10]). Zr K-edge EXAFS (extended x-ray absorption fine structure) results [8] are consistent with these observations. Other workers [11] have suggested that for $0.3 < x < 0.5$ the local structure is similar to $ZrSiO_4$, but $ZrSiO_4$ contains only isolated SiO_4 tetrahedra [3], which is completely inconsistent with ^{29}Si NMR observations of $(ZrO_2)_x(SiO_2)_{1-x}$ xerogels [8].

This paper reports a combined x-ray and neutron diffraction and Zr K-edge EXAFS and XANES (x-ray absorption near edge structure) study of $(ZrO_2)_x(SiO_2)_{1-x}$ xerogels, with $0.1 \leqslant x \leqslant 0.4$. The effect of the ZrO_2 content on the structure of the xerogels and on the Zr local environment is investigated.

2. Method

2.1. Sample preparation

The $(ZrO_2)_x(SiO_2)_{1-x}$ xerogel samples were prepared using precursors of zirconium n-propoxide, $Zr(OPr^n)_4$ (Aldrich, 70 wt% in propan-1-ol), and tetraethyl orthosilicate, TEOS (Aldrich, 98%). Because the reactivity of $Zr(OPr^n)_4$ is much greater than that of TEOS, the TEOS was pre-hydrolysed before the addition of the $Zr(OPr^n)_4$ [12]. In addition, the $Zr(OPr^n)_4$ was further diluted in propan-1-ol to prevent precipitation of ZrO_2 phases. The dilution used in this study, i.e. 1:30, was greater than in our previous study, i.e. 1:4 [8], in order to increase the homogeneity of the Zr distribution in the xerogels. Pre-hydrolysis was carried out by mixing together TEOS, propan-1-ol and water in the molar ratio of 1.0:1.3:2.0 for approximately 1 h. The diluted $Zr(OPr^n)_4$ was then added to the TEOS mixture. The samples were allowed to dry in air, leaving friable, clear xerogels.

The $(ZrO_2)_x(SiO_2)_{1-x}$ xerogel samples were prepared with ZrO_2 contents of $x = 0.1$, 0.2, 0.3 and 0.4. The densities and compositions of the samples are listed in table 1. The compositional information was determined using the results of ICP-AES, thermogravimetric analysis and calibrated solid-state NMR. The densities were measured using the Archimedes method with 2-butanol as the buoyant liquid. The xerogel samples contain residual quantities of solvent. All of the samples are amorphous.

Table 1. Densities and compositions of $(ZrO_2)_x(SiO_2)_{1-x}$ xerogels. (All uncertainties are ±10% relative to the stated value.)

	Density	Composition (at%)				
x	(g cm^{-3})	Si	Zr	O	C	H
0.1	1.66	12.3	1.4	36.8	10.2	39.3
0.2	1.86	10.4	2.5	36.2	10.1	40.8
0.3	1.99	8.5	3.6	35.5	10.0	42.4
0.4	2.18	6.6	4.7	34.9	9.9	43.9

Several reference compounds were examined in the XANES experiments: $ZrSiO_4$ (Strem Chemicals); yttria-stabilized tetragonal and cubic ZrO_2 (st-ZrO_2 and sc-ZrO_2 respectively)

and m-ZrO_2 (Tosoh Corporation) and $Zr(OH)_4$, and $Zr(OPr^n)_4$ (Aldrich, 70 wt% in propan-1-ol). The $Zr(OH)_4$ sample was prepared by the precipitation method: zirconium choride octahydrate dissolved in distilled water was mixed with ammonia solution. The precipitate was washed with water and filtrated, then heated to 230 °C to remove excess water

2.2. X-ray diffraction

X-ray diffraction experiments were carried out on Station 9.1 of SRS, Daresbury Laboratory. The data were collected from powdered samples using the transmission mode with θ–2θ geometry. Incident x-rays of wavelength $\lambda = 0.485$ Å were used, corresponding to a large Q range (up to 22 $Å^{-1}$), where $Q = 4\pi \sin(\theta)/\lambda$ is the modulus of the scattering vector. X-rays of this wavelength (energy of ∼25.6 keV) will excite fluorescence in Zr atoms (Zr K-edge energy of ∼18.0 keV), and the fluorescent x-rays would cause a large background signal. This was avoided by using the Warren–Mavel method [13]. The energy of the incident x-rays was chosen to be slightly more than the Ag K-edge (i.e. 25.5 keV), and a Ag foil was placed at the 2θ scattering position. The spectrum due to, primarily, elastically scattered x-rays was measured from the fluorescence of the Ag foil using a detector 13 mm away and set at 45 ° to the scattered beam.

The measured scattering intensity is corrected for detector dead time, intensity variation of the incident beam, polarization of the incident beam, θ dependence of the sample volume illuminated, background scattering and absorption. After normalizing to the theoretical self-scattering, the scattering intensity in electron units, I_{eu}, is obtained [14]. The structural information is described by the total structure factor:

$$S(Q) = 1 + \frac{I_{eu} - (N \sum_i c_i f_i^2)}{N \bar{f}^2} \tag{1}$$

where the term in brackets is the self-scattering. The other parameters are the number of atoms N, the elemental concentrations c_i, and the elemental and average scattering factors f_i and $\bar{f}$, respectively, which are Q-dependent. Note that f_i are determined from theoretical calculations of atomic electron distributions, and if these do not accurately reflect the real atomic electron distributions, systematic errors are introduced.

The measured $S(Q)$ is a sum of contributions due to correlations between different pairs of elements i and j (e.g. Si–O) [14]:

$$S(Q) = \sum_i \sum_j \left(\frac{c_i f_i c_j f_j}{\bar{f}^2} \right) S_{ij}(Q) \tag{2}$$

where each contribution is described by a partial structure factor, $S_{ij}(Q)$, and the ratios in brackets are weighting factors, w_{ij}. For an amorphous material (i.e. an isotropic scatterer) the relationship between the structure factor, and correlations between pairs of atoms is [15]

$$Q(S(Q)) - 1) = \int_0^\infty 4\pi r \rho_0 (g(r) - 1) \sin(Qr)\, \mathrm{d}r \tag{3}$$

where ρ_0 is the average atomic number density, and $g(r)$ is the pair distribution function. In this work we report results using the standard structural function

$$t(r) = 4\pi r \rho_0 g(r) \tag{4}$$

which is obtained by Fourier transform of $S(Q)$. For an i–j correlation (e.g. Si–O) with a Gaussian distribution of distances, the contribution to $S_{ij}(Q)$ is [15]

$$\Delta S_{ij}(Q) = \frac{N_{ij} w_{ij}}{c_j} \frac{\sin(QR_{ij})}{QR_{ij}} \exp(-\sigma_{ij}^2 Q^2/2) \tag{5}$$

where N_{ij} is the coordination number (type j atoms around a type i atom), R_{ij} is the mean distance and σ_{ij} is the standard deviation.

Structural information can be obtained by comparing the experimental results with a model generated using a sum of terms from equation (5) representing different i–j correlations. The experimental and model $S(Q)$ are Fourier transformed to generate $t(r)$, and the $t(r)$'s are compared. The parameters N_{ij}, σ_{ij} and R_{ij} are iterated and the procedure repeated until the best fit to the experiment is achieved. In this way, the same Fourier transform effects apply to the experimental data and model fits. A Hanning window function was used in the Fourier transform, to reduce the truncation effects due to limited Q range.

2.3. Neutron diffraction

Neutron diffraction experiments were carried out using the LAD diffractometer [16] at ISIS, Rutherford Appleton Laboratory, UK. Each powdered sample was placed inside a cylindrical vanadium can with a diameter of 6 mm. Data was collected up to Q values of 35 Å^{-1}. This larger Q range provides a greater resolution in real space compared with the x-ray diffraction data. Unfortunately there was insufficient quantity of the $x = 0.1$ sample remaining to obtain satisfactory neutron diffraction data.

The data were corrected for detector dead time, intensity variation of the incident beam, background scattering, absorption and multiple-scattering scattering [16]. Inelastic scattering corrections are commonly derived using the Placzek method [17]. These corrections are valid for relatively heavy nuclei, but are less reliable for light elements such as H. Since the $(ZrO_2)_x(SiO_2)_{1-x}$ xerogels studied here contain significant quantities of H, Placzek corrections could not sensibly be used. Instead, inelastic scattering contributions were removed by fitting Chebyshev polynomials to isolate the differential scattering cross section $\mathrm{d}\sigma/\mathrm{d}\Omega$. From this, the total structure factor is obtained,

$$S(Q) = 1 + \frac{\mathrm{d}\sigma/\mathrm{d}\Omega - (N\sum_i c_i b_i^2)}{N\bar{b}^2} \tag{6}$$

where the term in brackets is the self-scattering, and b_i and $\bar{b}$ are the elemental and average scattering lengths, respectively, which are independent of Q. Unfortunately, the method used to remove the effects of inelastic scattering may reduce the reliability of $S(Q)$.

The total structure factor obtained from neutron diffraction has analogous properties to that obtained from x-ray diffraction, except that the weighting factors w_{ij} depend on the scattering lengths b instead of the scattering factors f. This means that neutron and x-ray diffraction tend to emphasize different correlations. Structural information can be obtained in the same way as for x-ray data, i.e. equations (2)–(5) apply.

2.4. EXAFS

X-ray absorption spectroscopy experiments were carried out on Station 9.2 of the SRS, Daresbury Laboratory, UK. A Si(220) monochromator was used, with the harmonic rejection rate set at 50%. Samples with suitable optical thickness were prepared from the powders. The data were collected at the Zr K-edge (17 998 eV) in the transmission mode using standard ion chambers. The energy calibration was monitored using a third ion chamber and a Zr foil. Data was collected up to k values of 15 Å^{-1}, where k is the wavevector associated with the free photoelectron. Initial data processing was performed using the Daresbury Laboratory programs EXCALIB and EXBACK [18] to obtain the absorption μ. The EXAFS spectra are

given by [19],

$$\chi(k) = \frac{\mu(k) - \mu_{post}(k)}{\mu_{pre}(k) - \mu_{post}(k)} \tag{7}$$

where $\mu_{pre}(k)$ and $\mu_{post}(k)$ are fits to the pre- and post-edge backgrounds.

In single scattering, curved wave theory, $\chi(k)$ has the form [20]

$$\chi(k) = \sum_j S_0^2(k)|f_j(k, R_j)| \exp(-2R_j/\lambda(k)) \sin(2kR_j + 2\delta(k) + \varphi_j(k, R_j)) \exp(-2\sigma_j^2 k^2) \tag{8}$$

where N_j is the number of atoms at a distance R_j from the central absorbing atom, and $2\sigma_j^2$ is the Debye–Waller factor taking into account the structural and thermal disorder. Other parameters are the phase shifts due to the central excited atom, $\delta(k)$, and the back-scattering atom, $\varphi_j(k)$; the backscattering amplitude, $|f_j(k, R_j)|$; and the inelastic mean free path of the photoelectron, $\lambda(k)$. The amplitude reduction factor, $S_0^2(k)$, takes into account many-body effects.

To extract structural information, the experimental $\chi(k)$ is fitted using equation (8). EXCURV92 [18, 21] was used with Hedin–Lundqvist potentials and the relaxed atom approximation. To verify the suitability of this procedure, the experimental $\chi(k)$ was fitted for sc-ZrO_2 [10]. In this way the value of S_0^2 was determined to be 1.00 ± 0.05, and this value was used for the analysis of xerogel samples. The parameter E_f allows for errors in determination of the energy scale [19], and was free to vary in the fitting.

The parameters N_j, R_j, and $2\sigma_j^2$ were obtained by least squares fitting of $\chi(k)$ in k space with k^3 weighting. The $\chi(k)$ includes a non-EXAFS feature at $\sim$7.7 Å^{-1} which is attributed to a double electron transition [22]. Consequently, the data between 7.0 and 8.3 Å^{-1} was excluded during the fitting process. Because the parameters R_j and E_f and N_j and $2\sigma_j^2$ are correlated [23], the statistical errors were estimated from the 95% confidence level as a function of both fitted parameters in a pair. The statistical errors underestimate the uncertainty of the results when systematic errors are also present. The quality of fits can be judged from the discrepancy index

$$R_{dis} = \frac{\sum_i k_i^3 |\chi(k_i)_{data} - \chi(k_i)_{fit}|}{\sum_i k_i^3 |\chi(k_i)_{data}|}. \tag{9}$$

2.5. XANES

The XANES experiments were carried out on EXAFS Station 9.2 as described above. XANES spectra were collected in the near-edge region, from −15 to +30 eV with steps of 0.6 eV relative to the absorption edge. The limited lifetime of the core–hole causes a broadening of $\sim$2 eV at the Zr K-edge [24]. XANES spectra are presented in the form of $1 + \chi(E)$, where the energy scale E is set to zero at the inflection point of the main absorption edge ($E_0 = 17998$ eV). XANES spectra were collected for the xerogels samples and several reference compounds (see section 2.1). For the $Zr(OH)_4$ sample, the combined x-ray diffraction/EXAFS Station 9.3 was used. The experimental conditions were similar to those described above except that the XANES spectra were collected with steps of 1.7 eV.

3. Results

3.1. Expected interatomic correlations

The diffraction data includes regions of overlapping interatomic correlations which can only be interpreted by making assumptions. For $x = 0.1$, the SiO_2 network is dominant, and the

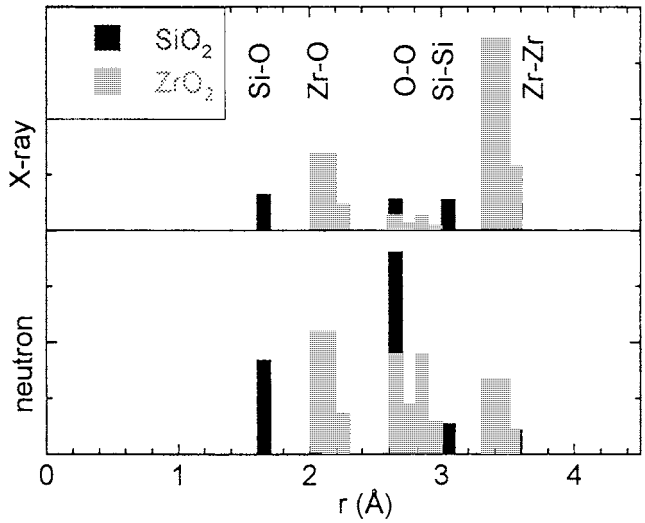

Figure 1. Estimated intensity of interatomic correlations for x-ray and neutron diffraction of SiO_2 and m-ZrO_2.

expected correlations can be estimated from the structure of SiO_2 [25]. For $x = 0.4$, there is a phase separation of ZrO_2, and the expected correlations can be estimated from the structure of m-ZrO_2 [9]. The expected intensities of these correlations are indicated in figure 1. Whereas SiO_2 has well defined O–O correlations at 2.63 Å, m-ZrO_2 has O–O correlations extending from 2.6 to 2.9 Å with a static disorder of $\sigma_{O-O} = 0.13$ Å. The latter can be neglected for $x = 0.1$, but will significantly overlap O–Si–O and Si–O–Si correlations for $x = 0.4$. Such O–Zr–O correlations are expected even if there is no phase separation of ZrO_2. Not shown are Zr–O–Si correlations which were observed at distances of 3.5–3.7 Å in minerals [26] and glasses [27], and 3.0 and 3.6 Å in $ZrSiO_4$ [3]. Also not shown are Si–O–Si–O correlations which begin at ∼3.5 Å and reach a maximum at ∼4 Å [25].

3.2. Diffraction results

The $Q(S(Q) - 1)$ obtained from x-ray and neutron diffraction are shown in figures 2 and 3, respectively. In both cases, it can be seen that $S(Q)$ is strongly increasing for $Q < 1$ Å^{-1}. This corresponds with the onset of small-angle scattering. Small-angle scattering occurs due to the microporous structure of Zr–Si xerogels, and also due to phase separation of ZrO_2 in xerogels with large x. We have previously presented small-angle x-ray scattering results on $(ZrO_2)_x(SiO_2)_{1-x}$ xerogels [28].

The $t(r)$ obtained from x-ray diffraction is shown in figure 4. Structural parameters were obtained from model fits (see figures 2 and 4) and are shown in table 2. The Si–O and Zr–O correlations are observed in $t(r)$ at 1.6 and 2.1 Å respectively. Additional peaks in $t(r)$ at ∼2.6 and ∼3.0 Å were fitted with O–O and Si–Si correlations, respectively. The peak at ∼3.5 Å is at the distance expected for Zr–O–Zr and Zr–O–Si correlations (see section 3.1). Although Zr–O–Zr and Zr–O–Si correlations overlap, the former will be dominant for large x (because there is phase separated ZrO_2 and Zr scatters more strongly than Si), and the latter will be dominant at small x (because there is no phase-separated ZrO_2 and the Zr content is smaller). Hence, the peak at ∼3.5 Å was fitted using Zr–Si correlations for $x = 0.1$ and 0.2, and Zr–Zr correlations for $x = 0.3$ and 0.4.

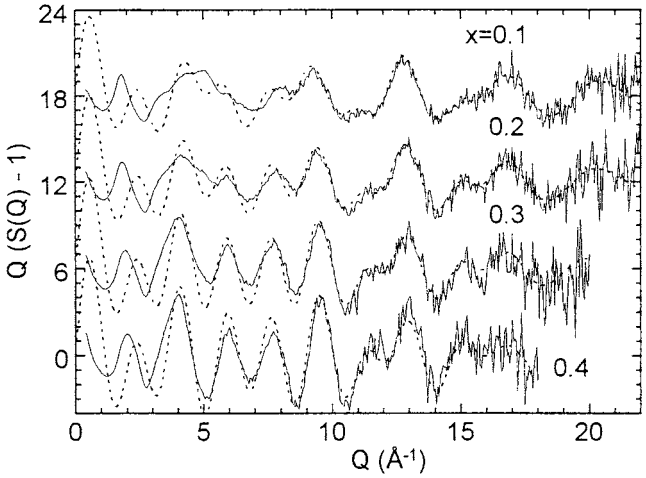

Figure 2. X-ray diffraction $Q(S(Q)-1)$ for $(ZrO_2)_x(SiO_2)_{1-x}$ xerogels with $x = 0.1$, 0.2, 0.3 and 0.4. The broken curves show model fits.

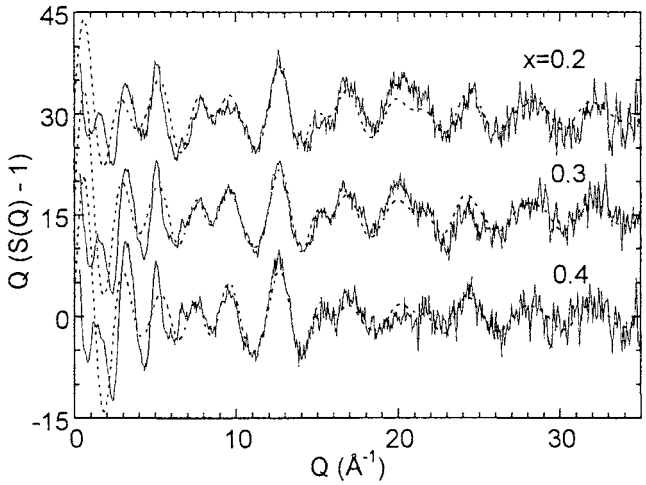

Figure 3. Neutron diffraction $Q(S(Q)-1)$ for $(ZrO_2)_x(SiO_2)_{1-x}$ xerogels with $x = 0.2$, 0.3 and 0.4. The broken curves show model fits.

The $t(r)$ obtained from neutron diffraction is shown in figure 5. Structural parameters were obtained from model fits (see figures 3 and 5) and are shown in table 3. The Si–O, Zr–O and O–O correlations are observed in $t(r)$ at 1.6, 2.1 and 2.6 Å respectively. In addition, the $t(r)$ were fitted with Si–Si correlations at ∼3.0 Å. The fits also include peaks at ∼3.5 Å representing Si–Zr and Zr–Zr correlations, as for x-ray diffraction, but these are not well defined due to the large features in $t(r)$ at $r > 3.5$ Å.

The $t(r)$ from neutron diffraction show a strong peak at ∼2.6 Å corresponding to O–O correlations. However, $t(r)$ in the region from 2.4 to 2.8 Å cannot be adequately fitted using a single peak. A single peak gives the wrong shape for $t(r)$, and would require unreasonably large peaks to be used for the Zr–O and Si–Si correlations at 2.1 and 3.0 Å respectively. This is almost certainly due to the difference between O–Si–O and O–Zr–O correlations, both of

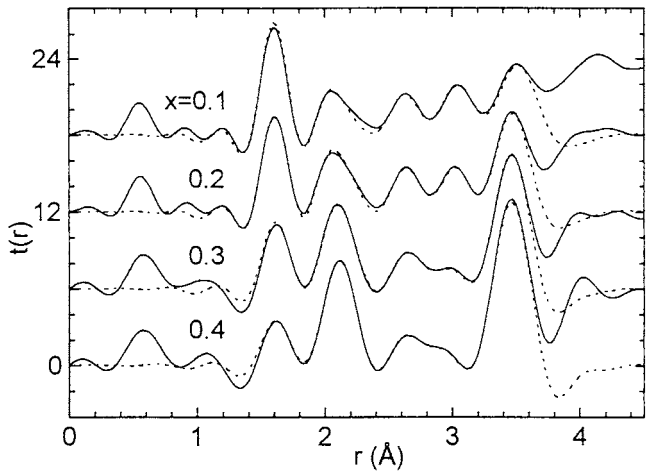

Figure 4. X-ray diffraction $t(r)$ for $(ZrO_2)_x(SiO_2)_{1-x}$ xerogels with $x = 0.1$, 0.2, 0.3 and 0.4. The broken curves show model fits.

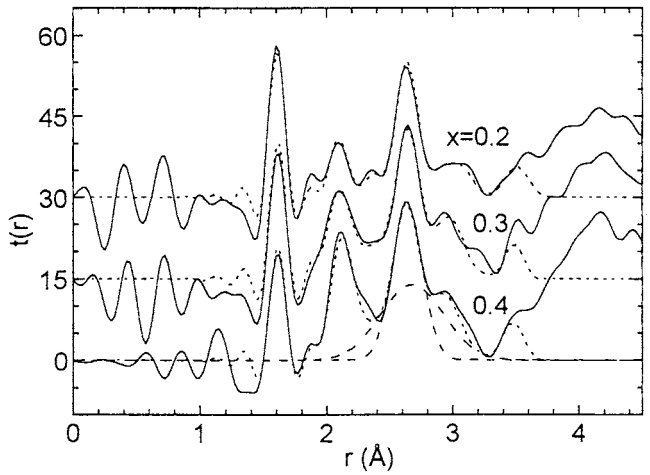

Figure 5. Neutron diffraction $t(r)$ for $(ZrO_2)_x(SiO_2)_{1-x}$ xerogels with $x = 0.2$, 0.3 and 0.4. Dotted lines show model fits.

which contribute to the observed O–O correlation (see section 3.1). Hence $t(r)$ in the region from 2.4 to 2.8 Å was fitted using a sum of two O–O correlations, i.e. O–Oa and O–Ob (see table 3). The comparison between the latter and a single O–O correlation is illustrated in figure 5 for the case of $x = 0.4$.

3.3. EXAFS and XANES results

The $k^3\chi(k)$ and Fourier transform $|k^3\chi(k)|$ obtained from EXAFS are shown in figures 6 and 7. The Fourier transforms show features at ∼1.5 Å which are unphysical, being too short for a realistic values of R_{Zr-O}. Other workers have observed similar artefacts in Zr and Ti K-edge EXAFS [22, 29]. Structural parameters were obtained from model fits (see figures 6 and 7) and are listed in table 4. The lowest discrepancy indexes, R_{dis}, were obtained by

Table 2. Structural parameters obtained from the model fitting of x-ray diffraction $t(r)$ for $(ZrO_2)_x(SiO_2)_{1-x}$ xerogels.

	Si–O			Zr–O			O–O		
x	N (±0.4)	R (Å) (±0.02)	σ (Å) (±0.005)	N (±0.8)	R (Å) (±0.02)	σ (Å) (±0.015)	N (±0.5)	R (Å) (±0.02)	σ (Å) (±0.01)
0.1	3.7	1.61	0.045	6.7	2.07	0.125	4.8	2.63	0.1
0.2	4.0	1.61	0.040	6.3	2.08	0.130	5.2	2.64	0.09
0.3	3.9	1.62	0.030	6.0	2.10	0.120	5.0	2.66	0.08
0.4	3.9	1.63	0.025	6.3	2.11	0.110	4.7	2.66	0.07
	Si–O–Si			Si–O–Zr			Zr–O–Zr		
x	N (±1.0)	R (Å) (±0.03)	σ (Å) (±0.02)	N (±2)	R (Å) (±0.04)	σ (Å) (±0.02)	N (±1.0)	R (Å) (±0.04)	σ (Å) (±0.03)
0.1	5.6	3.05	0.13	13	3.51	0.15	—	—	—
0.2	6.2	3.03	0.12	9	3.4	0.13	—	—	—
0.3	5.4	3.00	0.11	—	—	—	5.9	3.46	0.15
0.4	6.4	2.97	0.1	—	—	—	5.8	3.46	0.14

Table 3. Structural parameters obtained from the model fitting of neutron diffraction $t(r)$ for $(ZrO_2)_x(SiO_2)_{1-x}$ sol–gel samples. Note that the O–O correlation was fitted using the sum of two peaks, i.e. O–Oa and O–Ob.

	Si–O			Zr–O			O–Oa O–Ob		
x	N (±0.4)	R (Å) (±0.01)	σ (Å) (±0.005)	N (±0.8)	R (Å) (±0.02)	σ (Å) (±0.01)	N (±0.3) (±0.05)	R (Å) (±0.015) (±0.02)	σ (Å) (±0.01) (±0.04)
0.2	3.8	1.61	0.035	6.0	2.09	0.070	2.4	2.64	0.065
							3.2	2.65	0.26
0.3	3.7	1.62	0.030	8.0	2.10	0.10	2.0	2.64	0.070
							5.2	2.68	0.26
0.4	3.4	1.62	0.025	7.5	2.13	0.095	1.8	2.63	0.075
							5.5	2.68	0.25
	Si–O–Si			Zr–O–Si			Zr–O–Zr		
x	N (±1.5)	R (Å) (±0.03)	σ (Å) (±0.02)	N (±3)	R (Å) (±0.04)	σ (Å) (±0.02)	N (±1.5)	R (Å) (±0.04)	σ (Å) (±0.02)
0.2	5.8	3.05	0.09	10	3.51	0.09	—	—	—
0.3	6.4	3.01	0.07	—	—	—	6.5	3.49	0.07
0.4	6.5	2.99	0.08	—	—	—	5.5	3.48	0.08

fitting a single Zr–O correlation for an $x = 0.4$ sample and two Zr–O correlations, i.e. Zr–Oa and Zr–Ob, for samples with $x < 0.4$. Only Zr–O–Zr next-nearest-neighbour correlations could be reliably identified. The same trends occurred in our previous EXAFS study of $(ZrO_2)_x(SiO_2)_{1-x}$ xerogels [8]. Our previous study [8] included ^{17}O NMR results which show the presence of Zr–O–Si configurations in all samples. Hence the inability to identify Zr–O–Si correlations in EXAFS indicates a limitation of EXAFS for these kinds of materials. Other workers have commented that Zr K-edge EXAFS can have reduced sensitivity to Zr–O–Si correlations [27].

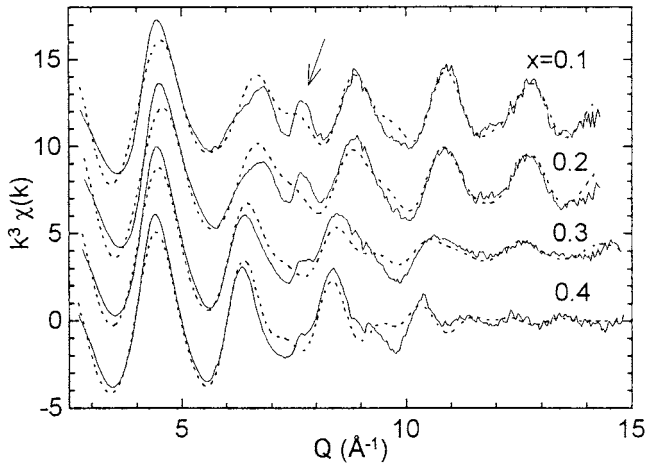

Figure 6. EXAFS $k^3\chi(k)$ for $(ZrO_2)_x(SiO_2)_{1-x}$ xerogels with $x = 0.1$, 0.2, 0.3 and 0.4. The broken curves show model fits. The arrow indicates a non-EXAFS feature attributed to a double electron transition [22].

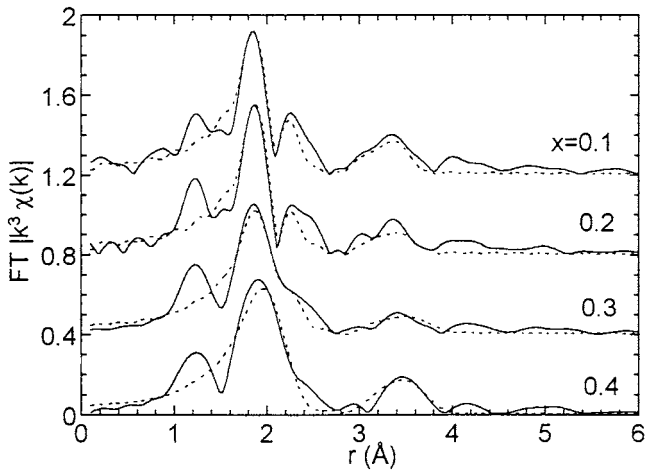

Figure 7. EXAFS Fourier transformed $|k^3\chi(k)|$ for $(ZrO_2)_x(SiO_2)_{1-x}$ xerogels with $x = 0.1$, 0.2, 0.3 and 0.4. The broken curve show model fits.

The XANES spectra of $(ZrO_2)_x(SiO_2)_{1-x}$ xerogels are shown in figure 8. Also shown are the XANES spectra of reference compounds. XANES at the K-edge involves the excitation of a 1s photo-electron into low-lying, empty states with p-type symmetry at the metal atom [30, 31]. Pre-edge features (see left arrow) correspond to empty states with p–d mixing which can occur for non-centrosymmetric metal atom sites. The shape of the main absorption peak represents transitions to np continuum states and 'shape resonances' of the metal atom site [30]. Peaks occurring a few tens of electronvolts above the edge (see right arrow) correspond to multiple scattering involving strongly-ordered, next-nearest-neighbour atoms. Qualitative information can be obtained by comparing the XANES spectra of the xerogels with those of the reference compounds (the so-called 'fingerprint' method) (e.g. [32]).

Table 4. Structural parameters obtained from the model fitting of EXAFS $k^3\chi(k)$ for $(ZrO_2)_x(SiO_2)_{1-x}$ xerogels. The asterisks denote results from our previous study of $(ZrO_2)_x(SiO_2)_{1-x}$ xerogels [8], in which a lower dilution of $Zr(OPr^n)_4$ in propan-1-ol was used (see section 2.1). The numbers in brackets are uncertainties in the last digits.

	Zr–Oa			Zr–Ob		
x	N	R (Å)	$2\sigma^2$ (Å^2)	N	R (Å)	$2\sigma^2$ (Å^2)
0.1	2.5(3)	2.01(1)	0.006(2)	5.0(9)	2.20(2)	0.026(6)
0.2	1.9(2)	2.01(1)	0.005(1)	5.5(10)	2.17(1)	0.034(7)
0.3	1.5(2)	2.03(1)	0.008(2)	5.5(6)	2.16(1)	0.026(4)
0.4	—	—	—	7.1(7)	2.12(1)	0.026(6)
0.1*	3.1(4)	2.00(1)	0.006(1)	6.4(13)	2.25(1)	0.031(9)
0.2*	—	—	—	9.5(9)	2.14(1)	0.038(4)
0.3*	—	—	—	8.4(6)	2.14(1)	0.029(3)
0.4*	—	—	—	7.9(5)	2.14(1)	0.023(2)

	Zr–Zr			
x	N	R (Å)	$2\sigma^2$ (Å^2)	R_{dis} (%)
0.1	1.1(5)	3.34(2)	0.017(7)	30
0.2	0.7(3)	3.37(2)	0.016(6)	34
0.3	2.4(11)	3.46(3)	0.033(10)	37
0.4	3.4(15)	3.48(2)	0.029(9)	35
0.1*	0.7(4)	3.37(1)	0.012(6)	35
0.2*	3.4(15)	3.53(3)	0.032(17)	39
0.3*	4.9(22)	3.50(1)	0.033(8)	35
0.4*	4.2(15)	3.49(1)	0.025(5)	30

4. Discussion

4.1. SiO_2 *network*

The values of R_{Si-O} and N_{Si-O} agree with those expected, i.e. 1.61 Å and 3.9, respectively [25]. The neutron data show that R_{Si-O} is independent of x, but the x-ray data show an increase in R_{Si-O} with increasing x. The latter is likely to be an artefact due to the presence of the large Zr–O peak at 2.1 Å. Both neutron and x-ray data show a decrease in disorder with increasing x, i.e. σ_{Si-O} decreases with increasing x,and this is unlikely to be an artefact. It implies that distribution of Zr in the absence of phase separation causes more distortion of the SiO_2 network than phase separation of ZrO_2 for large x.

In pure amorphous SiO_2 the O–Si–O and Si–O–Si correlations occur at $R_{O-O} = 2.63$ Å and $R_{Si-Si} = 3.08$ Å with $N_{O-O} = 5.9$ and $N_{Si-Si} = 4.0$ [25], but these decrease as SiO_2 is depolymerized. Our previous ^{29}Si NMR study of ZrO_2–SiO_2 xerogel samples [8] indicated the average number of non-bridging oxygens per SiO_4 tetrahedra increases from $\approx$0.5 for $x = 0.1$ to $\approx$1.0 for $x = 0.4$. Hence for $x = 0.1$ the expected coordination numbers are $N_{O-O} \approx 5.3$ and $N_{Si-Si} \approx 3.5$. The x-ray diffraction results for the $x = 0.1$ sample are dominated by the SiO_2 network, and are in reasonable agreement with those expected. For $x > 0.1$, the interpretation of O–O correlations is complicated by the overlap of O–Si–O and O–Zr–O correlations (see sections 3.1 and 4.2).

The neutron and x-ray diffraction results for Si–O–Si correlations in samples with $x > 0.1$ show $N_{Si-Si} = 6.0 \pm 0.5$ independent of depolymerization, and R_{Si-Si} decreasing with increasing x. These trends are not physically reasonable for a SiO_2 network with increasing

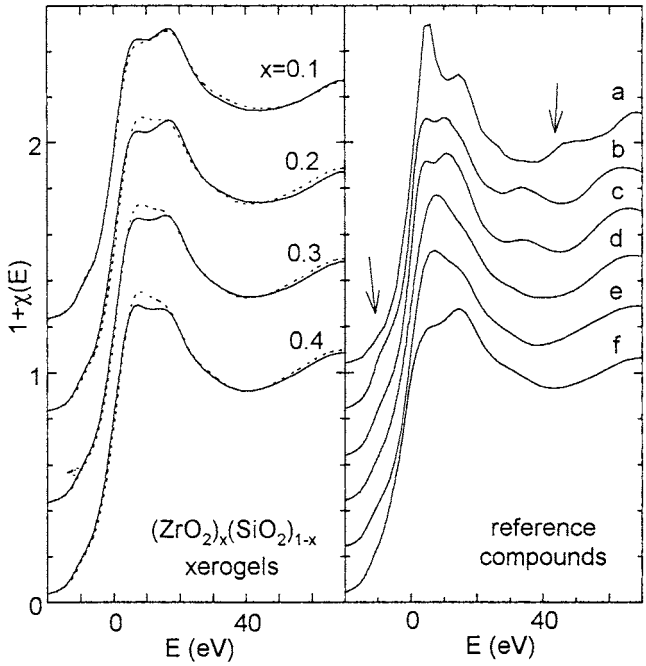

Figure 8. XANES $1 + \chi(E)$ for $(ZrO_2)_x(SiO_2)_{1-x}$ xerogels with $x = 0.1$, 0.2, 0.3 and 0.4 and reference compounds: (a) $ZrSiO_4$, (b) st-ZrO_2, (c) sc-ZrO_2, (d) m-ZrO_2, (e) $Zr(OH)_4$ and (f) $Zr(OPr^n)_4$. The left and right arrows indicate features due to p–d mixing and multiple scattering, respectively (see section 3.3). The broken curves represent the $(ZrO_2)_x(SiO_2)_{1-x}$ xerogels in our previous study [8], which had a less homogeneous Zr distribution than in this study due to lower dilution of Zr n-propoxide in propan-1-ol (see section 2.1).

depolymerization. This is almost certainly due to overlap with O–Zr–O correlations which increase with x, and can be expected to extend up to 2.9 Å (see sections 3.1 and 4.2).

4.2. Zr local environment

Both the neutron and x-ray diffraction data show $N_{Zr-O} = 6.7 \pm 0.8$ with no significant composition dependence, and R_{Zr-O} increasing with x from 2.08 Å for $x = 0.2$ to 2.12 Å for $x = 0.4$. Although the x-ray results for $x < 0.3$ may be affected by the presence of the Si–O peak at 1.6 Å, the peaks are well separated in the neutron data, and the increase in R_{Zr-O} is considered to reflect real changes in the sample structure.

The EXAFS data also show a total $N_{Zr-O} = 7.2 \pm 0.8$ and a mean $R_{Zr-O} = 2.13 \pm 0.01$ Å independent of x. However, for $x < 0.4$ the Zr–O correlation is split, and the results form a trend with the ratios N_{Zr-Oa}/N_{Zr-Ob} and R_{Zr-Ob}/R_{Zr-Oa} decreasing as x increases from 0.1 to 0.3. Hence the results form a trend that corresponds to the change from non-phase-separated Zr for small x, to phase separation of ZrO_2 for large x. Note this trend of decreasing asymmetry is consistent with the increase in diffraction values of R_{Zr-O}. Our previous EXAFS study of $(ZrO_2)_x(SiO_2)_{1-x}$ xerogel samples [8] gave similar results and trends (see table 4). However, in that case a split Zr–O correlation was only observed for $x = 0.1$, reflecting a less-homogeneous Zr distribution in those samples (see section 2.1). The XANES results also show a trend with increasing x, and this trend occurs more slowly for the xerogel samples in this compared to the previous [8] study. This is further confirmation of the differences between these samples.

The O–Zr–O correlations overlap with O–Si–O and, to a lesser extent, Si–O–Si correlations. The effects of this can be seen in the diffraction results. The x-ray diffraction data show $N_{O-O} = 5.0 \pm 0.5$ independent of x and R_{O-O} increasing with x. This is not expected for an SiO_2 network with increasing depolymerization, and is almost certainly due to overlap of O–Zr–O with O–Si–O correlations. Two O–O correlations, i.e. O–Oa and O–Ob, were required to fit the neutron diffraction data. Again, this can reasonably be attributed to the presence of both Si–O–Si and O–Zr–O correlations. The observations that $R_{O-Oa} = 2.64 \pm 0.02$ Å independent of x and N_{O-Oa} decreases with decreasing x are consistent with O–Si–O correlations. For $x = 0.4$, which has phase-separated ZrO_2, the values of $N_{O-Ob} = 5.5 \pm 0.5$ and $R_{O-Ob} = 2.68 \pm 0.02$ Å can be compared with those expected for O–Zr–O correlations, e.g. NO–O = 8.5 and RO–O = 2.78 Å for m-ZrO_2 [9]. The former are somewhat smaller than the latter, which may indicate a ZrO_2 phase with reduced connectivity, for example hydrated ZrO_2, or may be due to overlap with Si–O–Si correlations (see section 4.1).

Next nearest neighbour Zr–O–Zr and Zr–O–Si correlations are expected at ∼3.5 Å. These cannot be separated, and the diffraction data was fitted by using Zr–O–Si correlations for $x = 0.1$ and 0.2 and Zr–O–Zr correlations for $x = 0.3$ and 0.4. For $x = 0.3$ and 0.4, the x-ray diffraction and EXAFS data show $R_{Zr-Zr} = 3.47 \pm 0.02$ Å with $N_{Zr-Zr} = 5.8 \pm 1.0$ and $N_{Zr-Zr} = 3.4 \pm 1.5$, respectively. The neutron diffraction data is consistent with this. There is a marked change in the EXAFS results for N_{Zr-Zr} and R_{Zr-Zr} between $x = 0.2$ and 0.3, which can be attributed to onset of phase separation of ZrO_2. For $x = 0.1$ and 0.2 the x-ray diffraction data gave $N_{Zr-Si} = 11 \pm 2$, which is too large. This suggests that we cannot neglect other contributions to $t(r)$ at ∼3.5 Å such as Si–O–Si–O and weak Zr–Zr correlations. Indeed, for $x = 0.1$ and 0.2, the EXAFS gives $N_{Zr-Zr} = 0.9 \pm 0.5$, indicating that there is some clustering of Zr even in the absence of phase separation.

The parameters obtained for xerogels can be compared with those for reference compounds, which are shown in table 5. For $x = 0.4$, which has phase-separated ZrO_2, it can be seen that $N_{Zr-O} = 7.0 \pm 0.8$, $R_{Zr-O} = 2.13 \pm 0.01$ Å and $R_{Zr-Zr} = 3.47 \pm 0.02$ Å give the best agreement with an environment like that in m-ZrO_2. This is consistent with our previous study [8]. The smaller observed Zr–O distance, i.e. 2.13 Å, compared to m-ZrO_2, i.e. 2.17 Å, has previously been attributed to the asymmetry of the Zr–O distances in m-ZrO_2 [33]. A similar Zr local environment has been proposed for $Zr(OH)_4$ [34]. The latter can be expected to have some similarity to the ZrO_2 phase in ZrO_2–SiO_2 xerogels because they are hydrated. The XANES spectra for $x = 0.4$ do not show a strong similarity to any of the reference samples. However, the XANES spectra show a trend with increasing x of increasing similarity to that for $Zr(OH)_4$. This trend is more evident for the xerogel samples in our previous study [8] which had a less homogeneous Zr distribution (see section 2.1).

For $x = 0.1$, the observed Zr–Oa correlation ($R_{Zr-Oa} = 2.01 \pm 0.01$ Å and $N_{Zr-Oa} = 2.5 \pm 0.3$) compares best with those in sc-ZrO_2 ($R_{Zr-Oa} = 2.04$ Å and and $N_{Zr-Oa} = 3$) [10] and $Zr(OPr^n)_4$ ($R_{Zr-Oa} = 1.94$ Å and $N_{Zr-Oa} = 2$) [35]. The Zr–Ob correlation ($R_{Zr-Ob} = 2.20 \pm 0.01$ Å and $N_{Zr-Ob} = 5.0 \pm 0.9$) also compares well. This is consistent with previous studies [7, 8], which indicated that the Zr nearest-neighbour environment in the absence of phase separation is similar to that in c-ZrO_2. In fact, both R_{Zr-Oa} and N_{Zr-Oa} are intermediate between the corresponding values for sc-ZrO_2 and $Zr(OPr^n)_4$. The XANES spectra for $x = 0.1$ shows most similarity to that for $Zr(OPr^n)_4$. The latter can be expected to have some similarity to Zr in ZrO_2–SiO_2 xerogels because $Zr(OPr^n)_4$ is the precursor. Furthermore, $Zr(OPr^n)_4$ consists of dimers with $N_{Zr-Zr} = 1$, which parallels the weak Zr–Zr correlation seen in the EXAFS results for $x = 0.1$ and 0.2. However, the larger values of total N_{Zr-O} and mean R_{Zr-O} imply a coordination of seven in the xerogel compared to six in

Table 5. Structural parameters for ZrO_2 reference compounds from crystallographic data and Zr K-edge EXAFS. The ideal forms of cubic and tetragonal ZrO_2 are only stable at high temperatures, and sc-ZrO_2 and st-ZrO_2 refer to yttria stabilized room-temperature forms, respectively [10]. Italics indicates parameters which were fixed during EXAFS fitting. The asterisks denote Zr–Si correlations. The numbers in brackets are uncertainties in the last digits.

	Zr–Oa Zr–Ob			Zr–Zr		
Compound	Crystal $N \times R$ (Å)	EXAFS $N \times R$ (Å)	A (Å^2)	Crystal $N \times R$ (Å)	EXAFS $N \times R$ (Å)	A (Å^2)
$ZrSiO_4$ [3, 8]	4 × 2.12	*4* × 2.12(1)	0.005(2)	2 × 3.00∗	*2* × 3.00(1)∗	0.005(2)*
	4 × 2.26	*4* × 2.26(1)	0.006(2)	4 × 3.64	*4* × 3.64(1)	0.006(1)
st-ZrO_2 [10, 8]	4 × 2.08	*4* × 2.09(1)	0.010(2)	12 × 3.62	*12* × 3.62(1)	0.018(1)
	4 × 2.38	*4* × 2.28(3)	0.05(2)			
sc-ZrO_2	3 × 2.04	*3* × 2.11(1)	0.008(1)	12 × 3.64	*12* × 3.60(1)	0.021(2)
([10], this study)	4 × 2.23	*4* × 2.21(1)	0.020(5)			
m-ZrO_2 [9, 8]	7 × 2.16	*7* × 2.13(1)	0.019(2)	7 × 3.45	*7* × 3.46(1)	0.013(1)
$Zr(OH)_4$ [34]	—	2.0(5) × 2.08(1)	0.010	—	1.7(10) × 3.27(3)	0.023
	—	5.0(5) × 2.16(1)	0.022	—	2.0(10) × 3.41(3)	0.023
$Zr(OPr^n)_4$	2 × 1.94	2.0(1) × 1.97(1)	0.007(2)	1 × 3.47	1.4(3) × 3.43(2)	0.007(3)
[35, 36]	4 × 2.17	4.0(1) × 2.19(3)	0.016(8)			

$Zr(OPr^n)_4$. This could occur if there is an additional long Zr–O bond, for example, to a water group. In fact, such ligands have been proposed for $Zr(OH)_4$ [34].

5. Conclusions

The $(ZrO_2)_x(SiO_2)_{1-x}$ xerogel samples in the present study have a more homogeneous Zr distribution than those in our previous study, due to greater dilution of the precursor $Zr(OPr^n)_4$ in propan-1-ol. The Zr–O and Zr–Zr correlations clearly show a change between one Zr local environment and another as x increases from 0.2 to 0.3, corresponding to the onset of phase-separated ZrO_2. A close comparison of the Zr local environment with those in reference compounds was made. For $x \geqslant 0.3$, the Zr environment in phase-separated ZrO_2 is similar to that in m-ZrO_2 and $Zr(OH)_4$. For $x \leqslant 0.2$ there is no phase separation, and the Zr–O correlation is split with two or three well defined, short Zr–O bonds at 2.00 Å, and five longer Zr–O bonds at 2.20 ± 0.02 Å. This Zr coordination is more similar to that in Zr-propoxide, rather than c-ZrO_2 as concluded in previous studies. There is some and Zr–Zr clustering, i.e. $N_{Zr-Zr} = 0.9 \pm 0.5$, and the Zr distribution causes distortion of the SiO_2 network.

Acknowledgments

We thank M G Tucker for help with sample preparation, G Bushnell-Wye, W S Howells and F J W Mosselmans for help with the x-ray and neutron diffraction, and EXAFS experiments respectively, and D M Pickup for helpful discussions. We would also like to thank the EPSRC for funding this work through various grants.

References

[1] Nogami M 1985 *J. Non-Cryst. Solids* **69** 415
[2] Kamiya K, Sakka S and Tatemichi Y 1980 *J. Mater. Sci.* **15** 1765

[3] Hazen R M and Finger L W 1979 *Am. Mineral.* **64** 157
[4] Evans A M, Williamson J P H and Glasser F P 1980 *J. Mater. Sci.* **15** 2325
[5] Brinker C J and Scherer G W 1990 *Sol-Gel Science* (San Diego: Academic)
[6] Gill R 1989 *Chemical Fundamentals of Geology* (London: Unwin Hyman) ch 9
[7] Lee S W and Condrate R A 1988 *J. Mater. Sci.* **23** 2951
[8] Pickup D M, Mountjoy G, Wallidge G W, Newport R J and Smith M E 1999 *Phys. Chem. Chem. Phys.* **1** 2527
[9] Smith D K and Newkirk H W 1965 *Acta Crystallogr.* **18** 983
[10] Li P, Chen I-W and Penner-Hahn J E 1993 *Phys. Rev.* B **48** 10 063
[11] Stachs O, Gerber T and Petkov V 1997 *J. Mater. Sci.* **32** 4209
[12] Yoldas B E 1980 *J. Non-Cryst. Solids* **38** 81
[13] Bushnell-Wye G, Finney J L, Turner J, Huxley D W and Dore J C 1992 *Rev. Sci. Instrum.* **63** 1153
[14] Warren B E 1990 *X-ray Diffraction* (New York: Dover)
[15] Gaskell P H 1991 *Materials Science and Technology Glasses and Amorphous Materials* vol 9, ed J Zrzycky (Weinhaim: VCH) ch 4
[16] Hannon A C, Howells W S and Soper A K 1990 *2nd Workshop on Neutron Scattering Data Analysis (IOP Conference Series, vol 107)* ed M W Johnson p 193
[17] Placzek F 1950 *Phys. Rev.* **86** 377
[18] Dent A J and Mosselmans J F W 1995 *A Guide to EXCALIB* (Daresbury Laboratory)
Dent A J and Mosselmans J F W 1995 *A Guide to EXBACK* (Daresbury Laboratory)
Dent A J and Mosselmans J F W 1995 *A Guide to EXCURV92* (Daresbury Laboratory)
[19] Sayers D E and Bunker B A 1988 *X-ray Absorption* ed D C Koningsberger and R Prins (New York: Wiley) p 211–53
[20] Crozier E D 1997 *Nucl. Instrum. Meth. Phys. Res.* B **133** 134
[21] Binsted N, Campbell J W, Gurman S J and Stephenson P C 1991 *CCLRC Daresbury Laboratory EXCURV92 Program*
[22] Wang W-C and Chen Y 1998 *Phys. Status Solidi* A **168** 351
[23] Joyner R W, Martin K J and Meehan P 1987 *J. Phys. C: Solid State Phys.* **20** 4005
[24] Teo B K 1986 *EXAFS: Basic Principles and Data Analysis* (Berlin: Springer) p 70
[25] Grimley D I, Wright A C and Sinclair R N 1990 *J. Non-Cryst. Solids* **119** 49
[26] Farges F, Brown G E and Velde D 1994 *Am. Mineral.* **79** 838
[27] Farges F, Ponader C W and Brown G E 1991 *Geochim. Cosmochim. Acta* **55** 1563
[28] Mountjoy G, Pickup D M, Wallidge G W, Holland M A, Newport R J and Smith M E 2000 *MRS 1999 Fall Meeting Symp. Proc.* accepted for publication
[29] Antonioli G, Lottici P P, Manzini I, Gnappi G, Montenero A, Paloschi F and Parent P 1994 *J. Non-Cryst. Solids* **77** 179
[30] Bianconi A 1987 *X-ray Absorption* ed D C Koningsberger and R Prins (New York: Wiley) ch 11
[31] Grunes L A 1983 *Phys. Rev.* B **27** 2111
[32] Brydson R, Garvie L A J, Craven A J, Sauer H, Hofer F and Cressey G 1993 *J. Phys.: Condens. Matter* **5** 9379
[33] Farges F, Ewing R C and Brown G E 1993 *J. Mater. Res.* **8** 1983
[34] Turrillas X, Barnes P, Dent A J, Jones S L and Norman C J 1993 *J. Mater. Chem.* **3** 583
[35] Vaatstra B A, Huffman J C, Gradeff P S, Hubert-Pfalzgraf G, Daran J-C, Parraud S, Yunlu K and Caulton K G 1990 *Inorg. Chem.* **29** 3126
[36] Reinohl U, Ertel T S, Horner W, Weber A and Bertagnolli H 1998 *Ber. Bunsenges. Phys. Chem.* **102** 144